2008

The Parsec-Scale Jets of the TeV Blazars H1426+428, 1ES 1959+650, and PKS 2155-304: 2001-2004

B. Glenn Piner
Whittier College, gpiner@whittier.edu

Niraj Pant

Philip G. Edwards

THE PARSEC-SCALE JETS OF THE TeV BLAZARS H1426+428, 1ES 1959+650, AND PKS 2155−304: 2001−2004

B. GLENN PINER,[1] NIRAJ PANT,[1] AND PHILIP G. EDWARDS[2]

ABSTRACT

We present Very Long Baseline Array (VLBA) observations of the TeV blazars H1426+428, 1ES 1959+650, and PKS 2155−304 obtained during the years 2001–2004. We observed H1426+428 at four epochs at 8 GHz and found that its parsec-scale structure consisted of a $\sim$17 mJy core and a single $\sim$3 mJy jet component with an apparent speed of $2.09c \pm 0.53c$. The blazar 1ES 1959+650 was observed at three epochs at frequencies of 15 and 22 GHz. Spectral index information from these dual-frequency observations was used to definitively identify the core of the parsec-scale structure. PKS 2155−304 was observed at a single epoch at 15 GHz with dual-circular polarization, and we present the first VLBI polarimetry image of this source. For 1ES 1959+650 and PKS 2155−304, the current observations are combined with the VLBA observations from our earlier paper to yield improved apparent speed measurements for these sources with greatly reduced measurement errors. The new apparent speed measured for component C2 in 1ES 1959+650 is $0.00c \pm 0.04c$ (stationary), and the new apparent speed measured for component C1 in PKS 2155−304 is $0.93c \pm 0.31c$. We combine the new apparent speed measurements from this paper with the apparent speeds measured in TeV blazar jets from our earlier papers to form a current set of apparent speed measurements in TeV high-frequency peaked BL Lac objects (HBLs). The mean peak apparent pattern speed in the jets of the TeV HBLs is about $1c$. We conclude the paper with a detailed discussion of the interpretation of the collected VLBA data on TeV blazars in the context of current theoretical models for the parsec-scale structure of TeV blazar jets.

Subject headings: BL Lacertae objects: individual (1ES 1959+650, H1426+428, PKS 2155−304) — galaxies: active — galaxies: jets — radio continuum: galaxies

1. INTRODUCTION

The field of TeV gamma-ray astronomy has grown rapidly over the past several years with the advent of sensitive new gamma-ray telescopes such as H.E.S.S. and MAGIC. Particularly interesting results have been obtained in blazar astronomy, as the total number of detected TeV blazars has increased from six only a few years ago to 17 this year (Wagner 2008a). The majority of the detected TeV blazars (16 of 17) belong to the class of high-frequency peaked BL Lac objects (HBLs)—so named because the two peaks in their spectral energy distribution (SED) occur at relatively high UV/X-ray and GeV/TeV energies. This two-peaked SED in HBLs is most commonly interpreted as the result of relativistic electrons (and possibly positrons) radiating in a jet that is undergoing bulk relativistic motion at a small angle to the observer's line of sight, with the low-frequency peak due to synchrotron radiation, and the high-frequency peak due to inverse Compton scattering of the jet's own synchrotron photons (synchrotron self-Compton [SSC] emission). The TeV source list is mostly limited to relatively nearby blazars ($z \lesssim 0.2$) because of the absorption of TeV gamma rays on the extragalactic background light.

The TeV observations have shown dramatic variability in a number of these blazars. Among the most remarkable variability events are the 200 s variability timescale detected for PKS 2155−304 in 2006 July by H.E.S.S. (Aharonian et al. 2007) and the 3 minute variations detected for Mrk 501 in 2005 June by MAGIC (Wagner 2008b). Such rapid variations suggest extremely small emitting volumes and/or time compression by large relativistic Doppler factors, e.g., $\delta \gtrsim 100$ for PKS 2155−304 (Aharonian

et al. 2007). High Doppler factors are also sometimes invoked in specific SSC models of TeV blazar spectra and variability; for example, Fossati et al. (2008) consider two SSC models to explain the X-ray/TeV variability of Mrk 421: one with $\delta \sim 20$ (scattering in the Klein-Nishina regime) and one with $\delta \sim 100$ (scattering in the Thomson regime). Such high Doppler factors are at the upper limit of what is expected in relativistic jets and challenge our understanding of these objects if they do in fact occur.

Complementary observations that are crucial to unraveling the physics of TeV blazar jets are provided by the VLBI technique, which yields radio images of the relativistic jets with subparsec resolutions for these nearby blazars. Apparent jet speeds, brightness temperatures, and limits on jet/counterjet brightness ratios can all be measured from VLBI images, and these quantities all provide constraints on fundamental jet parameters such as the bulk Lorentz factor and the angle of the jet to the line of sight (subject to some caveats discussed at length in § 4). Our understanding of the parsec-scale radio properties of the HBL class in general has been increased by the recent work of Giroletti et al. (2004a, 2006). Those authors studied a sample of low-redshift BL Lac objects with a variety of radio instruments and demonstrated that the radio properties of the HBLs are consistent with them being the beamed versions of nearby low-luminosity FR I radio galaxies. The TeV blazars thus likely have an intrinsically different parent population with weaker jets, compared to the more distant powerful blazars, which likely have FR II parents (e.g., Urry & Padovani 1995). The mean derived parsec-scale Lorentz factor for the HBL class by Giroletti et al. (2004a), including TeV sources, is only $\langle \Gamma \rangle \sim 3$, much lower than the Lorentz factors suggested by the TeV gamma-ray emission.

We have previously published a series of papers investigating the parsec-scale kinematic properties of TeV-detected HBLs through multi-epoch high-resolution VLBI observations, predominantly with the National Radio Astronomy Observatory's

[1] Department of Physics and Astronomy, Whittier College, Whittier, CA; gpiner@whittier.edu.
[2] CSIRO Australia Telescope National Facility, Narrabri NSW, Australia; philip.edwards@csiro.au.

VLBA,[3] and we extend that study in this paper. Previous papers in this series have included early VLBA and space VLBI observations of Mrk 421 (Piner et al. 1999); VLBI observations of Mrk 501 (Edwards & Piner 2002); VLBA observations of 1ES 1959+650, PKS 2155−304, and 1ES 2344+514 (Piner & Edwards 2004, hereafter Paper I); and new VLBA polarimetry observations of Mrk 421 (Piner & Edwards 2005). This fifth paper in the series adds new VLBA observations of the TeV blazars 1ES 1959+650 and PKS 2155−304, whose kinematics were relatively poorly determined in Paper I, as well as a four-epoch series of VLBA observations of H1426+428—the sixth TeV blazar to be discovered. Altogether we present six new images of 1ES 1959+650, four new images of H1426+428, and one new polarization image of PKS 2155−304, for a total of 11 new data sets. These data sets comprise the observations from our TeV blazar monitoring program over the years 2001–2004 (excepting the observations of Mrk 421, which were published separately in Piner & Edwards [2005]). Note that except for the two brightest sources (Mrk 421 and Mrk 501), the TeV blazars are too faint in the radio ($\lesssim 100$ mJy) to be included in other VLBA monitoring programs such as MOJAVE, and they typically require long observations to obtain images of sufficient dynamic range. Observational backgrounds on the three specific sources studied in this paper are presented in the results section for the specific source.

Our earlier work on the parsec-scale structure of TeV blazars has shown a noticeable lack of superluminal components in their jets, which contrasts with the rapid superluminal motions observed in the jets of more powerful blazars and with the high Lorentz factors derived from modeling the TeV emission. We have previously interpreted the general lack of superluminal components in HBLs as evidence for a lower bulk Lorentz factor in the parsec-scale radio-emitting region compared to the TeV-emitting region. Models that have been invoked to explain this "bulk Lorentz factor crisis" include jets that are decelerated along their length (Georganopoulos & Kazanas 2003; Wang et al. 2004; Bicknell et al. 2005), jets with transverse velocity structures consisting of a fast spine and a slower layer (Giroletti et al. 2004b; Ghisellini et al. 2005; Henri & Saugé 2006), or jets with opening angles large enough that unintentional averaging over multiple viewing angles (because of limited resolution) causes the apparent conflict (Gopal-Krishna et al. 2004; Gopal-Krishna et al. 2006). Finally, Gopal-Krishna et al. (2007) consider a combination of the last two models, i.e., large opening angle jets with transverse velocity structures. Some of these models may be distinguished through the observed statistical distribution of apparent speeds in TeV blazar jets (e.g., Gopal-Krishna et al. 2006), so we conclude the paper by presenting our current best set of TeV blazar apparent speed measurements from the complete series of five papers, which consists of 16 component speeds in six sources, and discussing the various models in the context of the current observations.

In this paper we use the cosmological parameters $H_0 = 71$ km s^{-1} Mpc^{-1}, $\Omega_m = 0.27$, and $\Omega_\Lambda = 0.73$ (Bennett et al. 2003). When results from other papers are quoted, they have been converted to this cosmology.

2. OBSERVATIONS AND DATA REDUCTION

We observed H1426+428 with the VLBA at 8.4 GHz at four epochs between 2001 July and 2003 October, under observation codes BE024 and BE029. A VLBI observation of H1426+428

had previously been made at 5 GHz by Kollgaard et al. (1996); however, our first observation (BE024 on 2001 July 4) was a pilot study to see whether H1426+428 had a parsec-scale jet that could be imaged at 8 GHz with the VLBA and to determine a more accurate position for the source. That observation was carried out in phase-referencing mode both to determine a milli-arcsecond (mas) level position and because the correlated flux density of H1426+428 was uncertain. The source J1419+3821, for which a submas position has been determined by the International Celestial Reference Frame (ICRF; Ma et al. 1998), was used as the phase-reference source. J1419+3821 has an angular separation of $4.6°$ from H1426+428.

We were able to model the phase-reference source, J1419+3821, with two circular Gaussian components: a 0.34 Jy unresolved core component and a 0.16 Jy component with a FWHM size of 1.2 mas located 0.6 mas to the south. Based on the ICRF position for J1419+3821, we derived a (J2000.0) position for H1426+428 of R.A. = $14^h28^m32.609^s$, decl. = $+42°40'21.05''$, which we expect to have an accuracy of better than 20 mas. With the use of this position, phase referencing was unnecessary in subsequent epochs, as fringes could be directly detected to H1426+428, with a correlated flux density of ~ 20 mJy at 8 GHz. Following the successful imaging of parsec-scale structure in H1426+428 in the pilot study, three further epochs were observed throughout 2003 (observation code BE029) to study the jet kinematics. All four observations recorded approximately 7 hr on-source, for an expected thermal noise limit of about 0.05 mJy beam^{-1}. Note that H1426+428 was observed at a lower frequency than the other sources in this paper and in Paper I, in order to achieve the needed sensitivity to image this fainter source.

1ES 1959+650 was observed with the VLBA during three 6 hr sessions between 2003 June and 2004 February, under observation code BE030. The observations were split between 15.4 and 22.2 GHz, with approximately 2.5 hr spent on-source at each frequency at each epoch (with approximately 1 hr of calibration scans and slewing). This source was observed at two frequencies in order to obtain spectral index information between the 15 and 22 GHz images and to help resolve potential ambiguities in the source structure discussed in Paper I. The 15 GHz data have been combined with the three epochs at this frequency from Paper I in order to obtain kinematic information over a six-epoch series for this source.

PKS 2155−304 was observed at a single 6 hr epoch on 2003 September 20 at 15.4 GHz, with dual-circular polarization, under observation code BE031. The goal of this observation was two-fold: to provide an additional epoch several years removed from the three epochs in Paper I, to better constrain the jet proper motion (which was poorly constrained in Paper I), and to produce the first VLBI polarimetry image of this source. Previous observations in Paper I had shown that the correlated flux density was large enough (at >100 mJy) to produce a useful polarization image at this frequency. Approximately 4 hr were spent on-source in this observation, with the additional 2 hr spent on polarization calibration sources.

An observation log of all new observations discussed in this paper is given in Table 1. All observations were recorded at a data rate of 128 Mbps. The AIPS software package was used for calibration and fringe fitting of the correlated visibilities, and the visibilities were edited and final CLEAN images produced using the DIFMAP software package. For the polarization experiment BE031, calibration of the polarization response of the feeds was done with `lpcal` in AIPS. The required electric vector position angle (EVPA) correction for BE031 was applied using `clcor` in

---

TABLE 1
OBSERVATION LOG

Source	Epoch	VLBA Observing Code	VLBA Antennas[a]	Frequency (GHz)	Time On-Source (hr)	Dual Pol.[b]
H1426+428	2001 Jul 4	BE024	All	8.4	7	No
	2003 Mar 22	BE029A	No SC	8.4	7	No
	2003 Jul 6	BE029B	All	8.4	7	No
	2003 Oct 19	BE029C	All	8.4	7	No
1ES 1959+650	2003 Jun 9	BE030A	No KP	15.4	2.5	No
	2003 Jun 9	BE030A	No KP	22.2	2.5	No
	2003 Oct 31	BE030B	All	15.4	2.5	No
	2003 Oct 31	BE030B	All	22.2	2.5	No
	2004 Feb 8	BE030C	All	15.4	2.5	No
	2004 Feb 8	BE030C	All	22.2	2.5	No
PKS 2155−304.................	2003 Sep 20	BE031	No BR	15.4	4	Yes

[a] BR = Brewster, Washington; KP = Kitt Peak, Arizona; and SC = St. Croix, US Virgin Islands.
[b] Whether or not the experiment recorded dual-circular polarization.

AIPS and was determined from the observed EVPA of calibrator source J2136+006 (which had a relatively stable EVPA during 2003), compared with the EVPA recorded for this source on the VLA/VLBA Polarization Calibration Page,[4] interpolated to our frequency and epoch of observation. Parameters for all images are given in Table 2; individual images are discussed in the results sections for the individual sources below. All data sets are shown restored with both uniform weighting (uvweight = 2, 0 in DIFMAP, improving resolution at the expense of signal-to-noise ratio [S/N]) and natural weighting (uvweight = 0, −2 in DIFMAP). None of the naturally weighted images have an rms noise level that significantly exceeds the expected thermal noise limit.

After final calibration of the visibilities, circular Gaussian model components were fit to the visibilities using the modelfit task in DIFMAP. Such models allow the structure of the jet to be described using only a few numerical parameters. The source structures in the images in this paper are relatively simple (partly due to the high resolution and limited dynamic range of these observations, and some of these sources show more complex

structures on lower resolution images that may not be well modeled as circular Gaussians), and in all cases satisfactory fits to the visibilities were obtained using only two circular Gaussian components (representing the core and one jet component). The model fits are given in Table 3, and results for each source are discussed in the results sections on the individual sources below. The reduced χ^2 for all model fits was under 1.0. Model fitting directly to the visibilities allows subbeam resolution to be obtained (e.g., Kovalev et al. 2005), and components can be clearly identified in the model fitting even when they appear blended with the core component in the CLEAN images.

As in Paper I, we estimate that these full-track observations allow us to fit positions of model component centers to within ∼10% of a uniform beam width, and this is the error assumed for subsequent analysis (calculated by taking 10% of the projection of the elliptical beam FWHM onto a line joining the center of the core to the center of the component). Error bars much larger than this result in fits to linear component motion that are so good as to be statistically unlikely, confirming that this estimated error is reasonable. Note that the low rms noise achieved by these long integrations allows us to detect even the faintest component (the 3 mJy component in H1426+428) with a S/N exceeding 30:1.

[4] See http://www.vla.nrao.edu/astro/calib/polar.

TABLE 2
PARAMETERS OF THE IMAGES

			NATURAL WEIGHTING			UNIFORM WEIGHTING		
SOURCE	EPOCH	FREQUENCY (GHz)	Beam[a]	Peak Flux Density (mJy beam⁻¹)	Lowest Contour[b] (mJy beam⁻¹)	Beam[a]	Peak Flux Density (mJy beam⁻¹)	Lowest Contour[b] (mJy beam⁻¹)
H1426+428	2001 Jul 4	8.4	1.54, 1.10, −4.9	20	0.13	1.07, 0.77, −7.4	18	0.28
	2003 Mar 22	8.4	2.17, 1.12, −19.2	19	0.12	1.63, 0.75, −20.7	19	0.22
	2003 Jul 6	8.4	1.80, 1.01, −7.9	16	0.11	1.30, 0.69, −8.7	15	0.20
	2003 Oct 19	8.4	1.77, 1.01, −5.2	16	0.11	1.26, 0.69, −4.4	15	0.19
1ES 1959+650	2003 Jun 9	15.4	0.97, 0.48, −4.3	107	0.37	0.74, 0.36, −2.4	98	0.67
	2003 Oct 31	15.4	1.01, 0.53, −6.1	104	0.35	0.75, 0.38, −5.2	95	0.55
	2004 Feb 8	15.4	1.12, 0.54, 5.3	77	0.36	0.77, 0.36, 1.3	67	0.70
	2003 Jun 9	22.2	0.65, 0.32, −1.6	101	1.09	0.52, 0.26, 0.8	92	1.68
	2003 Oct 31	22.2	0.72, 0.41, −1.0	84	0.78	0.53, 0.26, −0.6	76	1.38
	2004 Feb 8	22.2	0.85, 0.43, 10.5	61	0.72	0.56, 0.26, 10.0	52	1.41
PKS 2155−304...........	2003 Sep 20	15.4	1.92, 0.51, −11.0	122	0.38	1.30, 0.36, −7.8	110	0.77

[a] Numbers given for the beam are the FWHMs of the major and minor axes in milliarcseconds, and the position angle of the major axis in degrees. Position angle is measured from north through east.
[b] The lowest contour is set to be 3 times the rms noise in the image. Successive contours are each a factor of 2 higher.

TABLE 3
CIRCULAR GAUSSIAN MODELS

Source (1)	Epoch (2)	Frequency (GHz) (3)	Component (4)	S (mJy) (5)	r (mas) (6)	P.A. (deg) (7)	a (mas) (8)	χ_R^2 (9)	T_B (10^{10} K) (10)
H1426+428	2001 Jul 4	8.4	Core	19	...	...	0.22	0.96	0.8
			C1	4	1.02	−21.4	1.38		
	2003 Mar 22	8.4	Core	19	...	...	0.17	0.67	1.2
			C1	3	1.65	−26.8	1.46		
	2003 Jul 6	8.4	Core	16	...	...	0.19	0.64	0.8
			C1	3	1.60	−25.5	1.74		
	2003 Oct 19	8.4	Core	15	...	...	0.14	0.64	1.5
			C1	4	1.48	−23.9	2.03		
1ES 1959+650	2003 Jun 9	15.4	Core	81	...	...	0.07	0.72	10.0
			C2	72	0.34	124.0	0.55		
	2003 Oct 31	15.4	Core	81	...	...	0.09	0.72	5.9
			C2	58	0.32	125.5	0.62		
	2004 Feb 8	15.4	Core	63	...	...	0.15	0.73	1.5
			C2	46	0.41	129.8	0.51		
	2003 Jun 9	22.2	Core	90	...	...	0.09	0.58	2.6
			C2	72	0.33	124.2	0.48		
	2003 Oct 31	22.2	Core	82	...	...	0.13	0.59	1.2
			C2	35	0.42	126.5	0.54		
	2004 Feb 8	22.2	Core	59	...	...	0.15	0.55	0.7
			C2	30	0.46	126.7	0.47		
PKS 2155−304	2003 Sep 20	15.4	Core	130	...	...	0.23	0.68	1.4
			C1	15	1.04	163.9	0.48		

NOTE.—Col. (5): Flux density in millijanskys. Cols. (6) and (7): r and P.A. are the polar coordinates of the center of the component relative to the presumed core. Position angle is measured from north through east. Col. (8): a is the FWHM of the circular Gaussian component. Col. (9): The reduced χ^2 of the model fit. Col. (10): The maximum source-frame brightness temperature of the circular Gaussian core component is given by $T_B = (1.22 \times 10^{12})\{[S(1+z)]/a^2\nu^2\}$ K, where S is the flux density of the Gaussian in janskys, a is the FWHM of the Gaussian in mas, ν is the observation frequency in GHz, and z is the redshift.

Lower limits to the fitted core sizes (which yield upper limits to the measured brightness temperatures) were determined using the DIFWRAP program for model component error analysis (Lovell 2000). These size lower limits range from zero (completely unresolved components) to only about 20% less than the best-fit size, and they are discussed in the text on the core brightness temperature upper limits for each individual source below.

3. RESULTS ON INDIVIDUAL SOURCES

3.1. *H1426+428*

The detection in TeV gamma rays of the HBL H1426+428 by the Whipple, HEGRA, and CAT telescopes (Horan et al. 2002; Aharonian et al. 2002; Djannati-Ataï et al. 2002) made it the sixth HBL source to be detected in high-energy gamma rays, and at a redshift of $z = 0.129$, it was the most distant TeV HBL known at that time. Further analysis of the TeV gamma-ray emission is given by Petry et al. (2002) and Aharonian et al. (2003). Aharonian et al. (2003) and Costamante et al. (2003) consider various models for the absorption of gamma rays by the extragalactic background light and find that the data imply an intrinsic TeV spectrum that dominates the broadband SED. X-ray observations indicate that the synchrotron peak is sometimes located in excess of 100 keV (Costamante et al. 2001; Wolter et al. 2008) and that the location of the peak is significantly variable (Falcone et al. 2004). SSC models have been applied to the SED of H1426+428 by Wolter et al. (2008) and Costamante et al. (2003) (both using the one-zone homogeneous SSC model of Ghisellini et al. [2002]), and Kato et al. (2006); all of these models give Doppler and bulk Lorentz factors of about 20, and jet viewing angles of about 2°, but involve numerous assumptions.

VLA images of this source are shown by Laurent-Muehleisen et al. (1993) and Giroletti et al. (2004a). Laurent-Muehleisen et al. (1993) present a 1.5 GHz combined A- and C-configuration image that shows poorly represented diffuse emission north of the core. Giroletti et al. (2004a) detect the presence of a faint halo surrounding the central core, with a northeast extension oriented at P.A. $\sim 50°$, in their 1.4 GHz A-array image. H1426+428 has been previously observed with VLBI by Kollgaard et al. (1996) and by Giroletti et al. (2006). The 5 GHz Mk III VLBI image from 1991 by Kollgaard et al. (1996) shows a 2 mJy component 1.2 mas northeast (P.A. $\approx 20°$) of a 19 mJy compact core. The source is completely unresolved in the lower resolution 1.6 GHz European VLBI Network (EVN) image in Giroletti et al. (2006). Based on the available VLA and VLBI data, Giroletti et al. (2006) estimate a viewing angle of $\theta \sim 20°$ and a Doppler factor of $\delta \sim 3$, but those estimates are based on assumptions that may only be valid in a statistical sense for samples of many blazars (such as if the Lorentz factor $\Gamma \sim 1/\theta$).

Our four 8.4 GHz VLBA images of H1426+428 are shown in Figure 1. The top row of Figure 1 shows the naturally weighted images, while the bottom row shows the uniformly weighted images. Parameters of the images are given in Table 2. The linear resolution of these images at the distance of H1426+428 is approximately 2.3 pc mas^{-1}. The images all show a compact core with a flux density of ~ 17 mJy and a faint jet extending to the northwest, with a position angle of about $-25°$. The position angle of the extended structure seen at all four epochs is similar, and differs significantly from the position angle of the structure measured by Kollgaard et al. (1996) from their single 5 GHz Mk III VLBI image from 1991 of $\approx 20°$. No counterjet is detected; however, because of the low flux density of the jet, the limit that can
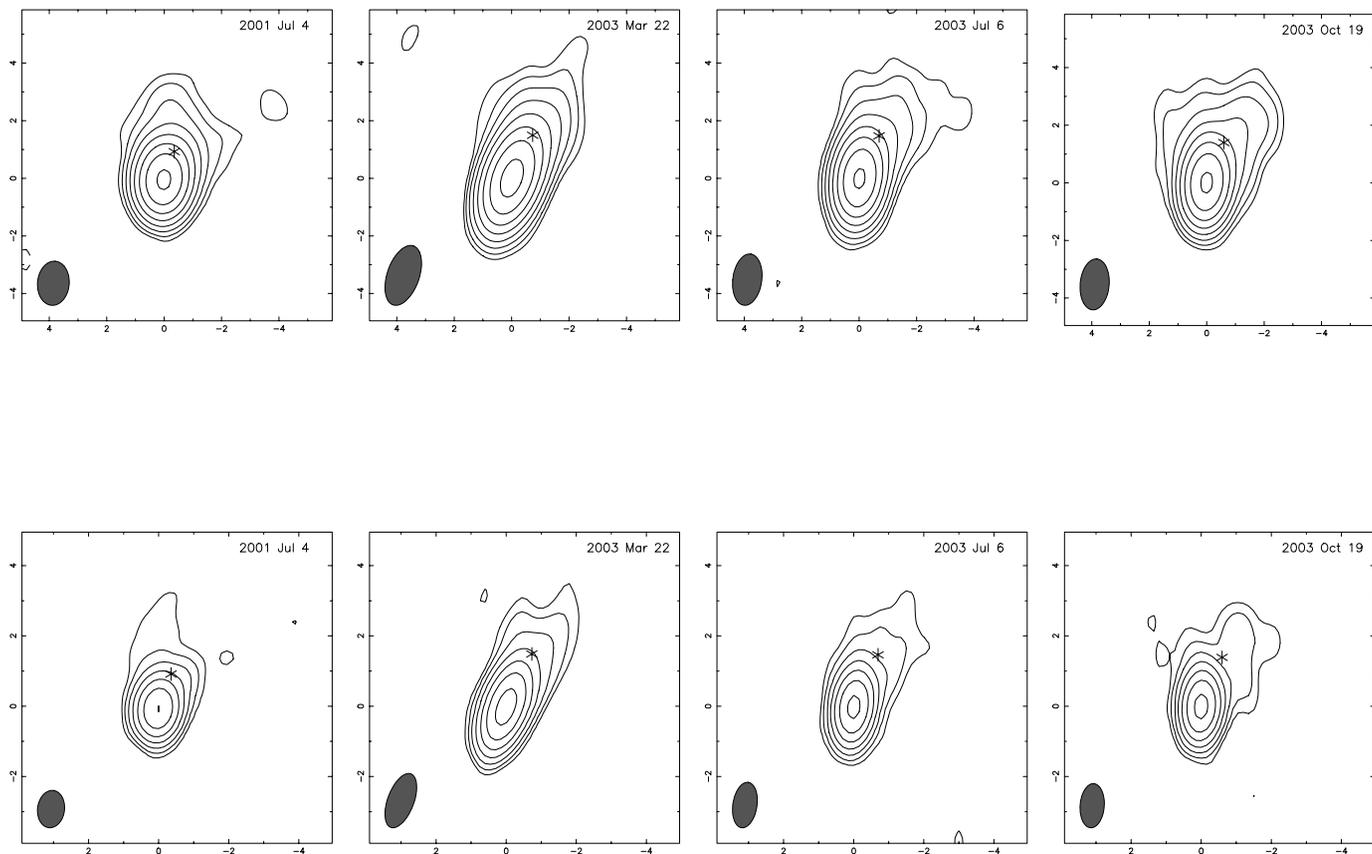
FIG. 1.—VLBA images of H1426+428 at 8.4 GHz. The top row shows the images obtained with natural weighting, while the bottom row shows the images obtained with uniform weighting. The axes are labeled in milliarcseconds (mas). Numerical parameters of the images are given in Table 2. The location of the center of the circular Gaussian (excluding the Gaussian representing the core) that was fit to the visibilities is marked with an asterisk. Parameters of the Gaussian models are given in Table 3.

be placed on the jet-to-counterjet brightness ratio is a rather low 30:1. Although variability and different resolutions may cause significant uncertainty, we can estimate a total VLBI spectral index between 1.6 (Giroletti et al. 2006), 5 (Kollgaard et al. 1996), and 8.4 GHz (this paper), and obtain $\alpha = -0.26 + 0.10$ ($S \propto \nu^{\alpha}$), a flat but not inverted spectral index.

The structure of H1426+428 at all four epochs is well modeled by two circular Gaussian components, representing the core and a single jet component, designated C1, with a flux density of about 3 mJy. Parameters of the Gaussian models are given in Table 3. The measured brightness temperature of the core is about 1×10^{10} K (see Table 3), but this component is unresolved (the visibilities are almost as well fit by a pointlike component), so that this brightness temperature should be considered a lower limit. The jet component appears to move out between 2001 and 2003, although no motion can be detected in the three 2003 epochs alone. A linear fit to the separation of the jet component from the core versus time is shown in Figure 2. The fit yields a measured apparent speed for the jet component of $2.09c \pm 0.53c$. Interpretation of model fitting data over only a few widely spaced epochs can lead to uncertainties in component identification (e.g., Piner et al. 2007), but for this source the structure is quite simple, minimizing the chances of confusing multiple components. If this measured apparent speed is taken as the bulk apparent speed of the jet[5] and is combined with the viewing angle

derived from SSC modeling of about $2°$ (see above), then the bulk Lorentz factor of the jet at the location of C1 is $\Gamma = 5.6$, and the Doppler factor is $\delta = 11$.

The difference of $45°$ in the position angle of the jet structure from that measured 12 years previously by Kollgaard et al. (1996) is interesting. Changes in position angles of component ejections have been well observed in other sources such as BL Lac and have been interpreted as periodic precession of the jet nozzle caused by binary supermassive black holes by some authors (e.g., Stirling et al. 2003; see also Mutel & Denn 2005). To find out whether or not such variations are occurring in H1426+428 will require waiting for the ejection of more components, because the two position angles measured 12 years apart are not enough to place any constraints on such a motion. We note that we do not detect any significant changes in the position angle of component C1 itself over the 2 years of monitoring covered in this paper (the change in the position angle of C1 of up to $5.4°$ in Table 3 corresponds to a transverse distance of only about 0.15 mas, about the size of the 1 σ positional error bars for this source).

3.2. *1ES 1959+650*

Observational background on the $z = 0.047$ HBL 1ES 1959+650 for results published prior to 2004 has been discussed in Paper I. Some more recent high-energy observational results include a spectral analysis of the 2002 TeV flares, including the "orphan" TeV flare in 2002 June (a TeV flare that occurred without a corresponding X-ray flare) by Daniel et al. (2005), and an analysis of low-level TeV emission detected by the MAGIC telescope in 2004 by Albert et al. (2006). Multiwavelength campaigns on

[5] The apparent jet speed $\beta_{app} = \beta \sin \theta / (1 - \beta \cos \theta)$, and the Doppler factor $\delta = 1/\Gamma(1 - \beta \cos \theta)$, where Γ is the bulk Lorentz factor, $\beta = v/c$, and θ is the angle to the line of sight.
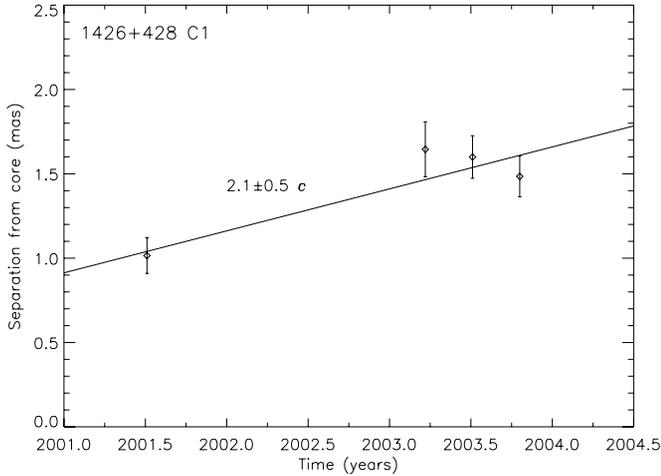
FIG. 2.—Distance from the core of the center of Gaussian component C1 in H1426+428 as a function of time. The line is the least-squares fit to outward motion with constant speed.

1ES 1959+650 from 2002 and 2003 are described by Krawczynski et al. (2004) and Gutierrez et al. (2006), respectively. Both of these papers model the multiwavelength SED of 1ES 1959+650 with a simple one-zone SSC model with a Doppler beaming factor of $\delta = 20$. Krawczynski et al. (2004) also discuss the difficulty of modeling the orphan flare mentioned above with conventional one-zone SSC models, and they suggest several alternatives, including multicomponent SSC models, external Compton models, and high-energy proton models. A specific model for producing orphan flares from relativistic protons is described by Böttcher (2005), but may require unreasonably high jet powers (Böttcher 2005). A multicomponent leptonic model that succeeds in producing orphan flares is described by Kusunose & Takahara (2006)

using an inhomogeneous conical jet geometry, with the line of sight inside the opening angle of the jet.

On the parsec scale, the 5 GHz VLBA images of 1ES 1959+650 by Rector et al. (2003) and Bondi et al. (2001, 2004) all show a diffuse jet with a broad ($\sim$55°) opening angle extending 20 mas north of the core along a position angle of $\approx$−5°. VLA images by Rector et al. (2003) and Giroletti et al. (2004a) show faint extended flux to both the north (P.A. $\approx$ −5°) and south (P.A. $\approx$ 175°) of the core, suggesting negligible Doppler boosting by the time the jet reached the arcsecond scale. Giroletti et al. (2006) estimate a viewing angle of $\theta \sim 20°$ and a Doppler factor of $\delta \sim 3$ on the parsec scale from the available radio data, similar to their result for H1426+428 discussed above.

Our three-epoch series of 15 GHz VLBA images of 1ES 1959+650 from 2003 to 2004 is shown in Figure 3, and the series of 22 GHz images from the same epochs is shown in Figure 4. Both sets of images are shown restored with both uniform and natural weighting. Parameters of these images are given in Table 2. At the redshift of 1ES 1959+650 ($z = 0.047$), the linear scale of the images is 0.9 pc mas^{-1}. These images can then be compared with our previous sequence of three 15 GHz VLBA images from 2000, as shown in Paper I. The 15 and 22 GHz images show a similar parsec-scale morphology, which is also similar to that seen for this source in Paper I, but markedly different from that seen in the lower resolution 5 GHz VLBA images by Rector et al. (2003) and Bondi et al. (2001, 2004). Figures 3 and 4 show a brighter, compact northwestern feature, with a short extension to the southeast along a position angle of $\approx$125°—this is particularly evident in the uniformly weighted 22 GHz images. This extension matches well the location of component C2 seen in Paper I. The diffuse northern jet seen in the 5 GHz VLBA images is only faintly present in the naturally weighted 15 GHz images. If we apply a taper to our 15 GHz VLBA data, then we better detect the diffuse northern emission. Figure 5 shows a tapered
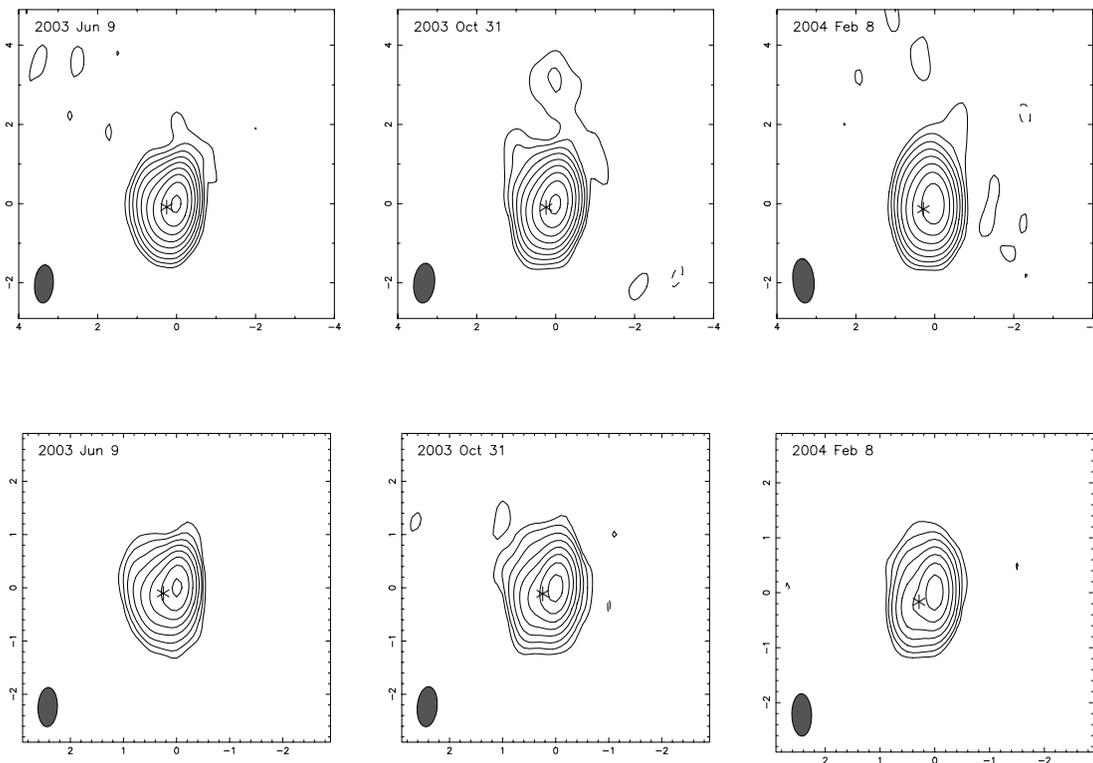

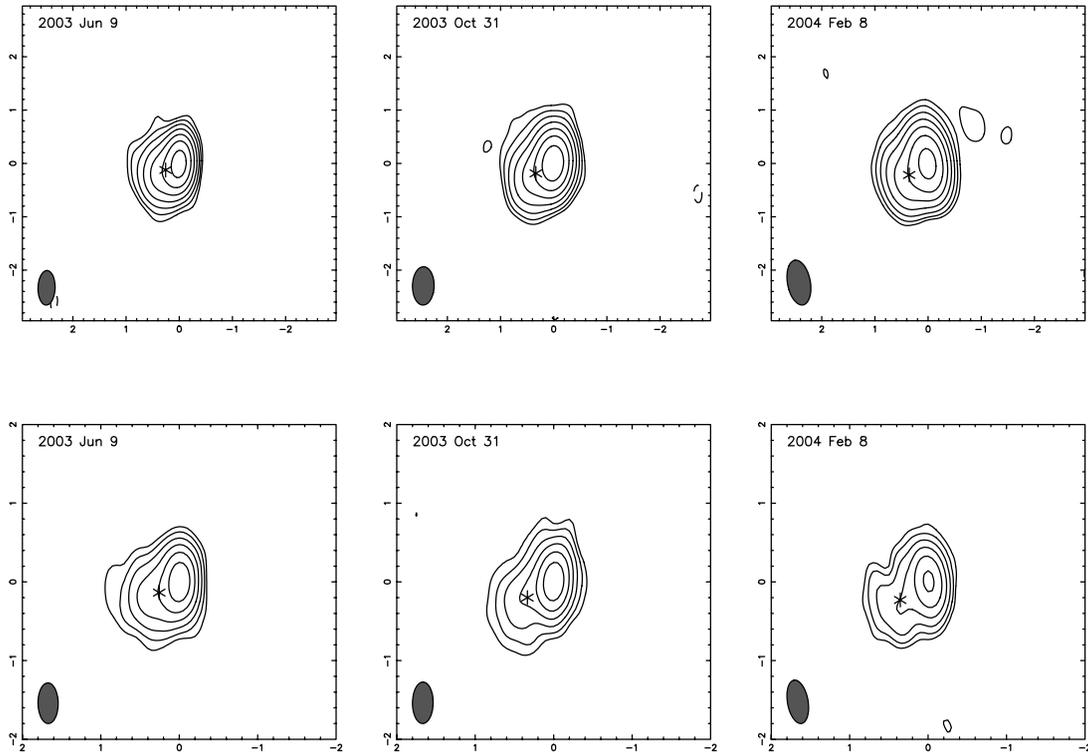FIG. 3.—Same as Fig. 1, but for VLBA images of 1ES 1959+650 at 15.4 GHz.

FIG. 4.—Same as Fig. 1, but for VLBA images of 1ES 1959+650 at 22.2 GHz.

image from our 15 GHz observation on 2004 February 8; parts of the northern jet are clearly visible, although at relatively low significance.

The morphology is intriguing because of the extreme misalignment between the parsec-scale structures seen at 5 GHz on the one hand, and 15 and 22 GHz on the other. If the northwestern
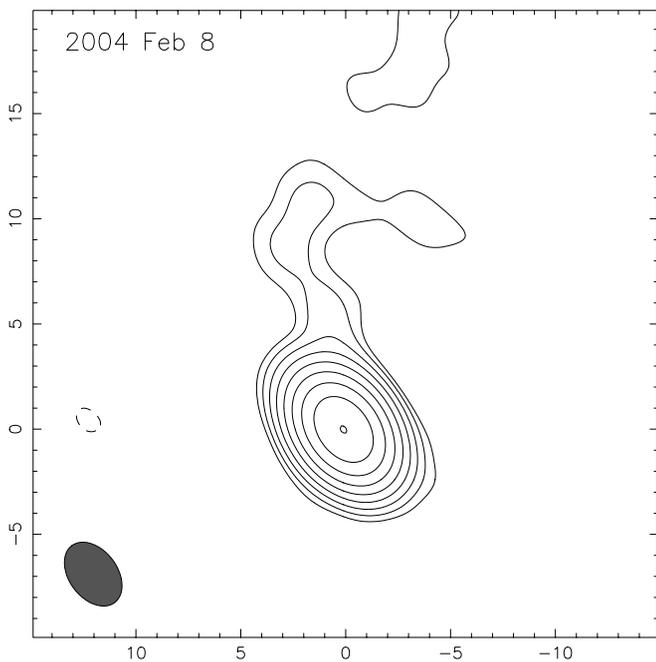

FIG. 5.—Tapered 15 GHz VLBA image of 1ES 1959+650 from 2004 February 8. The restoring beam is 3.39 mas by 2.3 mas at a position angle of 37°. The lowest contour is drawn at a flux density of 0.42 mJy beam^{-1} (3 times the rms noise level). Successive contours are each a factor of 2 higher. The peak flux density is 107 mJy beam^{-1}.

component on our images is the core (assumed in Paper I), then the jet starts to the southeast with a position angle of $\approx 125°$ at 0.5 mas from the core, before bending to a position angle of $\approx -5°$ at about 5 mas from the core. Such an extreme parsec-scale misalignment would most likely be due to a smaller intrinsic bend, amplified by projection effects caused by a small angle to the line of sight. Alternatively, the fainter southeastern feature could be the core, with the northwestern feature representing a brighter jet component, as has been seen in 4C 39.25 (e.g., Alberdi et al. 1993). Definitively identifying the core requires spectral information, which is obtained here from the dual-frequency 15 and 22 GHz observations. The core is expected to have an inverted or nearly flat spectral index due to synchrotron self-absorption, while the jet components are expected to have optically thin spectral indices.

A parsec-scale spectral index map of 1ES 1959+650 for the 2003 October 31 epoch is shown in Figure 6. The other two epochs yield similar spectral index maps. The map was constructed by restoring the 22 and 15 GHz images from that date with the same beam (using the average of the naturally weighted beams at each frequency) and calculating the spectral index at each pixel. The sign convention used is $S \propto \nu^{\alpha}$, where S is the flux density, ν is the observing frequency, and α is the spectral index. The northwest corner of the source has the flattest spectral index, with the spectral index steepening to the southeast, with a possible small rise again at the location of the stationary component C2. The spectral index map thus identifies the core as the brighter component at the northwest end of the source, as was assumed in Paper I, a result confirmed by the dual-frequency model fitting described below. This leaves a jet with an $\approx 130°$ apparent bend from the southeast to the north between 15 and 5 GHz VLBI scales as the most viable interpretation of the parsec-scale morphology.

The source visibilities are well modeled by two circular Gaussians at both frequencies; the parameters of these models are given in Table 3. The measured brightness temperature of the
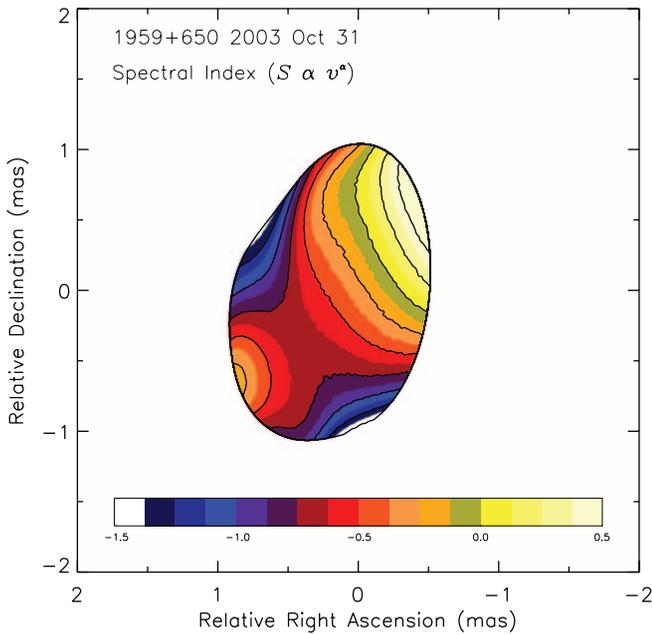
Fig. 6.—Spectral index map of 1ES 1959+650 between 15 and 22 GHz, on 2003 October 31. Contours are drawn from spectral indices of −1.5 to 0.5 in steps of 0.25. Spectral index is calculated as $S \propto \nu^{\alpha}$, where S is the flux density, ν is the observing frequency, and α is the spectral index. The spectral index has been plotted at all points where the flux density is at least 4 times the flux density of the lowest contour on the images at both frequencies, i.e., at least three contours up on both relevant images.

Fig. 7.—Distance from the core of the center of Gaussian component C2 in 1ES 1959+650 as a function of time. The line is the least-squares fit to outward motion with constant speed.

core component is a few $\times 10^{10}$ K, and it is partially resolved only at the final epoch at both frequencies, with a brightness temperature upper limit of 6×10^{10} K at both frequencies at that epoch. This is the same as the brightness temperature upper limit obtained for this source in Paper I. The jet component is blended with the core component on the CLEAN images, but because of its relatively high flux density relative to the core, it is highly significant in the model fitting. The location of this component matches well the expected location of the component labeled C2 in Paper I, so this component is subsequently referred to as C2 (but note that the same caveats discussed in the section on H1426+428 about the interpretation of model fitting data over widely spaced epochs still apply). The component labeled C1 in Paper I that appeared south of C2 at a separation of about 0.8 mas from the core and a position angle of 160° is no longer detected; presumably it has faded between 2001 and 2003. It is interesting to note that a larger and diffuse Gaussian component almost on top of the core is suggested by the model fitting, but not at a very significant level (so it is not included in Table 3), but we speculate that this may represent the older component C1 crossing almost over the core as the jet bends to the north.

The spectral indices of the two components can also be calculated from these dual-frequency model fits. We average the spectral indices calculated at all three epochs and obtain an average spectral index for the core of 0.04 ± 0.18, and an average spectral index for C2 of -0.85 ± 0.18, confirming the results obtained from the spectral index map. The errors on the spectral indices were calculated from an estimated 7% flux error at 15 GHz and an estimated 9% flux error at 22 GHz, where these estimated flux errors were obtained from the average correction applied by the `gscale` amplitude self-calibration routine in DIFMAP to the antenna amplitude scales. The average separation of component C2 from the core is slightly larger at 22 GHz than its average separation at 15 GHz (by 0.05 ± 0.04 mas), a result expected
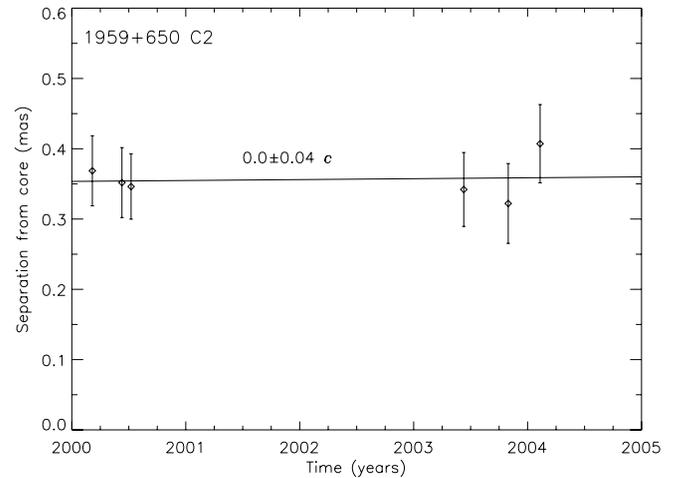
from inhomogeneous models of the radio core, where the "core" lies farther back along the jet at higher frequencies (e.g., Königl 1981). This measured frequency-dependent separation was compensated for in the spectral index map shown in Figure 6 by applying a relative shift in the proper direction to align component C2 between the two frequencies.

A linear fit to the separation of the jet component C2 from the core versus time from the six total 15.4 GHz images (three from this paper, three from Paper I) is shown in Figure 7. The fit yields a measured apparent speed for this component of $0.00c \pm 0.04c$, compared to a measured apparent speed of $-0.21c \pm 0.61c$ for this same component based on only the three epochs from 2000 that were analyzed in Paper I. The addition of the three new epochs thus lowers the upper limit on the apparent speed of this component by a factor of 10, from $0.40c$ to $0.04c$. Because of the low upper limit on the apparent speed, this component most likely represents a stationary component in the jet, whose apparent speed is not directly related to the bulk apparent speed of the jet (see the discussion on stationary and moving components in § 4). The flux density of the component is variable over the six epochs, as might be expected from a stationary feature with variable jet plasma passing through it. If only the three epochs from this paper are used in the fitting, then an apparent speed of $0.27c \pm 0.35c$ is obtained for the 15 GHz data, and an apparent speed of $0.59c \pm 0.29c$ is obtained from the 22 GHz data. We expect that these differences simply represent the uncertainty inherent in fitting an apparent speed from three epochs spaced over only half a year, and do not represent an actual acceleration of the component.

3.3. *PKS 2155−304*

The $z = 0.116$ HBL PKS 2155−304 is a prototypical object of this class and has been extensively observed at high energies. In particular, since 2002, its very high energy gamma-ray flux has been monitored with the H.E.S.S. array of atmospheric Cerenkov telescopes (Aharonian et al. 2005a). A multiwavelength campaign undertaken in 2003 is described by Aharonian et al. (2005b). These authors model the SED of this object during a low state, and fit the spectrum with several SSC model variations with Doppler boosting factors ranging between 25 and 50. Of particular note is the recent dramatic flaring activity at TeV energies on 2006 July 28 (Aharonian et al. 2007; Sakamoto et al. 2008). Bursts varying on timescales of 200 s were observed
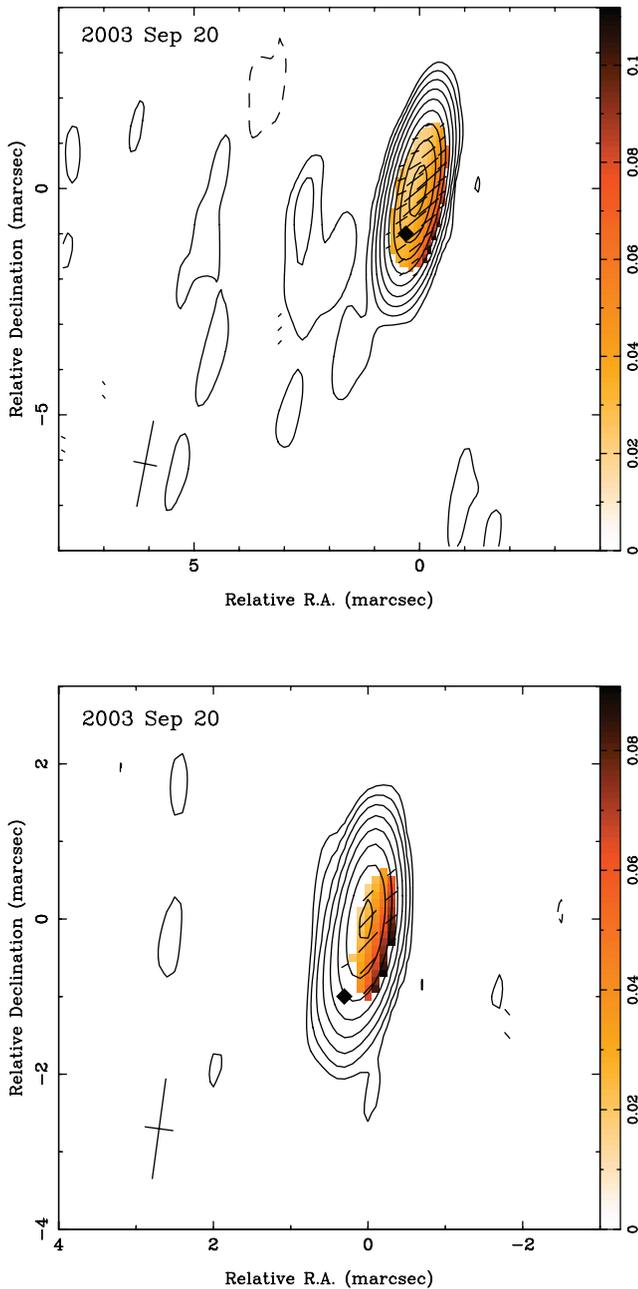
FIG. 9.—Tapered 15 GHz VLBA image of PKS 2155−304 from 2003 September 20. The restoring beam is 4.38 by 1.44 mas at a position angle of −4°. The lowest contour is drawn at a flux density of 0.45 mJy beam^{-1} (3 times the rms noise level). Successive contours are each a factor of 2 higher. The peak flux density is 140 mJy beam^{-1}.

FIG. 8.—VLBA images of PKS 2155−304 at 15.4 GHz. The top image is shown using natural weighting, while the bottom image is shown using uniform weighting. Numerical parameters of the images are given in Table 2. The location of the center of the circular Gaussian (excluding the Gaussian representing the core) that was fit to the visibilities is marked with a diamond. The tick marks show the magnitude of the polarized flux (with a scale of 0.2 mas mJy^{-1} in the top image, and 0.1 mas mJy^{-1} in the bottom image) and the direction of the EVPA. Tick marks are drawn at pixels where the polarized flux is greater than 3 times the rms noise in the polarization image. The colors show the fractional polarization, with the scale indicated to the right of the images.

during this outburst, requiring Doppler boosting factors greater than 100 if the emission region has a size comparable to the Schwarzschild radius of a $\sim 10^9 M_\odot$ black hole (Aharonian et al. 2007).

Probably because of its declination, this source has not been well observed in the radio. A series of images showing the large-scale radio structure of PKS 2155−304 is shown by Laurent-Muehleisen et al. (1993). The highest resolution VLA image presented by these authors shows a knot nearly 180° misaligned

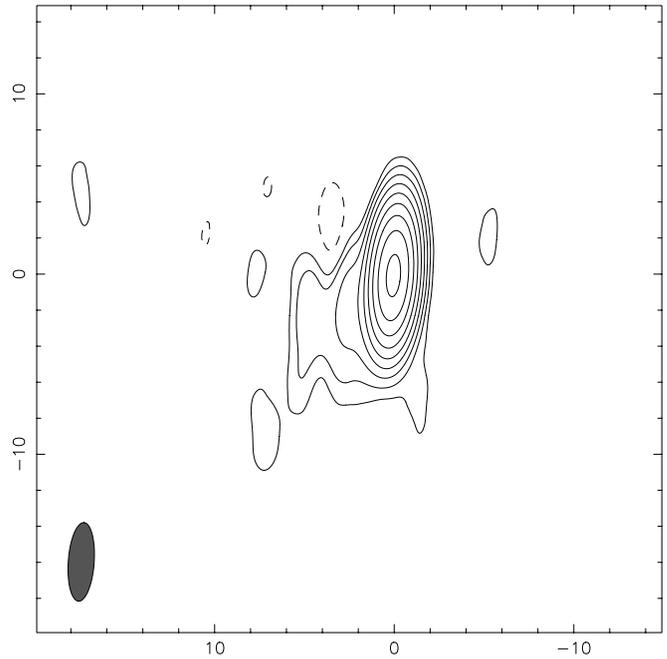from the VLBA jet seen in Paper I; the lower resolution VLA images by these same authors show an extended halo of emission around the core. This source has not been well observed with VLBI, and the only other published VLBI images known to us are the three-epoch set from Paper I.

Our new 15 GHz VLBA images of PKS 2155−304 from 2003 September 20 are shown in Figure 8. The linear resolution of these images at the distance of PKS 2155−304 is approximately 2.1 pc mas^{-1}. Parameters of these images are given in Table 2. The tick marks on the images indicate the magnitude of the polarized flux and the direction of the EVPA, and the color scale indicates the fractional polarization. These are the first parsec-scale polarization images of this object. The total-intensity morphology is consistent with that seen in Paper I, with a compact jet component to the southeast of the core (here at a position angle of $\approx 160°$), and a diffuse jet with a broad opening angle extending to the east. This diffuse eastern jet is more easily seen in the tapered image from the same data set shown in Figure 9.

Polarized flux is significantly detected at the location of the core component in both images in Figure 8. The percentage polarization at the model-fit position of the core (the origin) is 2.9%, and the electric vector position angle is 131°, about 30° misaligned from the innermost jet position angle. The fractional polarization increases to the west of the model-fit core position, to peak values of 8%−10% (see the color scale images in Fig. 8). Because the observations are at only a single frequency, no corrections have been made for Faraday rotation. However, the measured rotation measures in BL Lac objects are typically a few hundred rad m^{-2} or less (Zavala & Taylor 2003, 2004), resulting in an expected error of only about 10° or so to the EVPA at 15 GHz. The foreground integrated rotation measure in this region is low, resulting in a negligible correction of under 1° (Simard-Normandin et al. 1981).

As in Paper I, the visibilities are well fit by two circular Gaussians, consisting of the compact core and a single jet
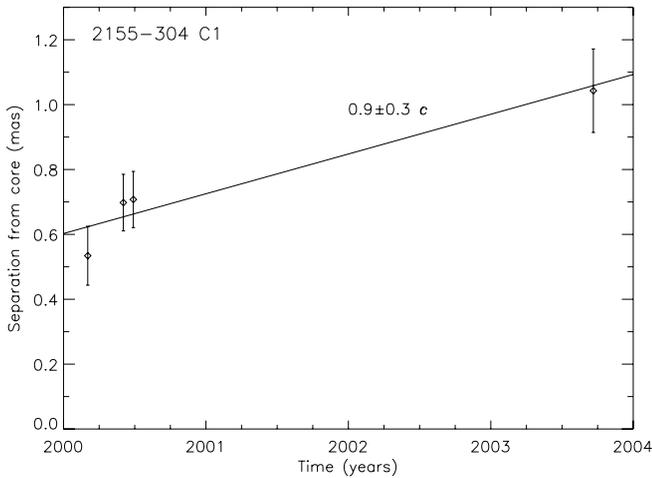
FIG. 10.—Distance from the core of the center of Gaussian component C1 in PKS 2155−304 as a function of time. The line is the least-squares fit to outward motion with constant speed.

component to the southeast of the core. Parameters of the model fit are given in Table 3. The core component is partially resolved with a best-fit size of 0.23 mas and a lower limit to its size of 0.19 mas, corresponding to an upper limit to its brightness temperature of 2×10^{10} K. The single jet component is slightly farther from the core than the jet component seen in Paper I, and we identify it as the same component, named C1 in Paper I. As mentioned above, identifying components across a several-year gap can be risky, but the structure of this source is simple, consisting of only a single jet component, so we consider this identification to be likely. A fit to the outward motion of this component using the combined four-epoch data set from this paper and Paper I is shown in Figure 10. The fitted apparent speed is $0.93c \pm 0.31c$. The measurement error on the apparent speed has been reduced by a factor of nearly 10 over the apparent speed given in Paper I of $4.37c \pm 2.88c$. The new apparent speed measurement is considerably lower than the previous value, but given the large associated error on the previous result, they are statis-

tically consistent at the 1.2 σ level. The component faded over the 3 years since it was first detected, from about 50 mJy in early 2000 (see Paper I) to about 15 mJy in 2003. It has also turned slightly to the south, moving from a position angle of $\approx 150°$ in 2000 to $\approx 160°$ in 2003.

4. DISCUSSION

A major data product resulting from the high-resolution multi-epoch VLBA monitoring is the apparent jet speeds. In Table 4 we give all apparent speeds that we have measured in TeV blazars over the course of our monitoring program. This table is meant to update Table 3 of Paper I, and it contains our results for Mrk 421 from Piner & Edwards (2005), as well as the new apparent speeds for H1426+428, 1ES 1959+650, and PKS 2155−304 measured in this paper. As noted in Paper I, the apparent pattern speeds measured in the TeV blazars are considerably slower than those measured in sources selected for their compact radio emission (Kellermann et al. 2004), or for their GeV gamma-ray emission (Jorstad et al. 2001). The updated apparent speed measurements added in this paper strengthen the statistical significance of these conclusions. Applying the Kolmogorov-Smirnov test to the apparent speed distribution in Table 4 compared to the apparent speed distributions in Kellermann et al. (2004) and Jorstad et al. (2001) shows that the TeV blazars have slower pattern speeds, with >99.75% confidence compared to the compact radio sources of Kellermann et al. (2004), and with >99.99% confidence compared to the EGRET blazars of Jorstad et al. (2001).

VLBA observations of the large 2 cm survey and MOJAVE survey have shown that powerful jets form VLBI patterns that move at apparent speeds ranging from zero up to the apparent bulk speed of the jet (Lister 2006; Cohen et al. 2007). These authors conclude that the peak apparent pattern speed measured in a jet from VLBI monitoring is then a good indicator of the apparent bulk speed of the flow. In the final column of Table 4, we therefore list the fastest pattern speed observed for each of these TeV blazars during our monitoring. All of these fastest speeds are below about $2c$, and four of the six are subluminal. One of the following two possibilities must then apply to the apparent pattern speeds in the parsec-scale jets of the TeV HBLs:

TABLE 4
APPARENT COMPONENT SPEEDS IN TeV HBLs

Source	Comp.	Apparent Speed[a] (Multiples of c)	Ref.	Fastest Apparent Speed (Multiples of c)
Mrk 421	C4	0.09 ± 0.07	1	0.10 ± 0.02
	C4a	-0.06 ± 0.09	1	. . .
	C5	0.10 ± 0.02	1	. . .
	C6	0.03 ± 0.03	1	. . .
	C7	0.06 ± 0.01	1	. . .
H1426+428	C1	2.09 ± 0.53	4	2.09 ± 0.53
Mrk 501	C1	0.05 ± 0.18	2	0.54 ± 0.14
	C2	0.54 ± 0.14	2	. . .
	C3	0.26 ± 0.11	2	. . .
	C4	-0.02 ± 0.06	2	. . .
1ES 1959+650	C1	-0.11 ± 0.79	3	0.00 ± 0.04
	C2	0.00 ± 0.04	4	. . .
PKS 2155−304.................	C1	0.93 ± 0.31	4	0.93 ± 0.31
1ES 2344+514	C1	1.15 ± 0.46	3	1.15 ± 0.46
	C2	0.46 ± 0.43	3	. . .
	C3	-0.19 ± 0.40	3	. . .

[a] For $H_0 = 71$ km s^{-1} Mpc^{-1}, $\Omega_m = 0.27$, and $\Omega_\Lambda = 0.73$.

REFERENCES.—(1) Piner & Edwards 2005; (2) Edwards & Piner 2002, with modified cosmological parameters; (3) Paper I; (4) this paper.

1. The pattern speeds are related to the bulk apparent speeds as described above, and the bulk apparent speeds are slower on the parsec scale in the TeV HBLs compared to the more powerful sources.

2. A much larger fraction (approaching 100%) of the HBLs have pattern speeds that are unrelated to their bulk apparent speeds than do the more powerful sources.

Either of these two possibilities implies a fundamental difference between the parsec-scale jets of HBLs and the more powerful sources, and we now discuss each possibility in turn.

4.1. *Pattern Speeds Related to Bulk Speeds*

If the fastest pattern speeds are an indication of the bulk apparent speed, as they are for the MOJAVE sources, then we have a typical bulk apparent speed of about $1c$ in the parsec-scale jets of the TeV blazars (the mean and median of the final column in Table 4 are both about $1c$). The bulk apparent speed is a function of the bulk Lorentz factor and the viewing angle, as is the Doppler factor (see equations in footnote 5). If the high Doppler factors implied by the high-energy observations are combined with the slow apparent speeds, then very small viewing angles are obtained (many under $1°$), which imply unreasonable numbers of parent objects (Henri & Saugé 2006). A statistically reasonable solution is then to adopt a lower Doppler factor (and therefore Lorentz factor) in the parsec-scale radio-emitting region than in the gamma-ray–emitting region. This argument was discussed in more detail in Paper I.

A lower Doppler factor and bulk Lorentz factor for the parsec-scale radio emission in HBLs is actually suggested by many observations other than the apparent pattern speeds. Each of the observables described below depends on the bulk Doppler factor of the jet, not on a pattern speed:

(*a*) The TeV blazars are significantly less variable in the radio band than are the EGRET blazars (Aller et al. 2006).

(*b*) The TeV blazars have low radio core brightness temperatures (see Table 3) that do not require invoking relativistic Doppler factors to reduce them below possible intrinsic limits. Typical high-power sources have much higher brightness temperatures (Kovalev et al. 2005; Dodson et al. 2008).

(*c*) The measured radio powers of the cores suggest Lorentz factors for HBLs of around $\Gamma = 3$, when this power is compared to that expected from the total power at low frequency (Giroletti et al. 2004a).

(*d*) The calculated inverse Compton Doppler factor from the VLBI cores of HBLs gives a mean lower limit to the Doppler factor of $\delta \gtrsim 4$, and a mean lower limit to the Lorentz factor of $\Gamma \gtrsim 2$ (see Table 7 in Giroletti et al. 2004a). Thus, high Lorentz factors are not required to reduce the predicted X-ray emission from the VLBI cores below the observed values.

(*e*) Optical and radio luminosities of HBLs could not be unified with their FR I parent population using only transverse jet velocity structures by Chiaberge et al. (2000), but the required properties could be reproduced by assuming that the radio-emitting region in HBLs is less beamed than the optical one, as could be expected if the jet decelerates after the higher energy emitting zone (Chiaberge et al. 2000).

(*f*) The VLBI jets of the TeV blazars assume a plumelike morphology beyond a few mas from the core, in contrast to high-power jets that may remain well collimated to large distances. This transition to a plumelike morphology has been interpreted as evidence for entrainment-induced deceleration in TeV blazars by Bicknell et al. (2005).

These six observational properties all imply relatively low bulk Doppler factors and Lorentz factors in these parsec-scale jets. It is clear that radio observations consistently yield Doppler factors and Lorentz factors for the TeV blazars (and HBLs in general) about an order of magnitude lower than the high-energy observations. However, arguing for a higher Lorentz factor is the fact that no counterjets have been observed in any of the TeV HBLs. Our observations put the limit on the jet-to-counterjet ratio J at $J \gtrsim 100$ for most of the sources. The tightest limits on J in a TeV blazar come from High Sensitivity Array (HSA) observations of Mrk 501 by Giovannini et al. (2008), which constrain $\beta \cos \theta > 0.92$, corresponding to $\Gamma \gtrsim 3$ for viewing angles of a few degrees. Thus, a parsec-scale Lorentz factor in the radio-emitting region of $\Gamma \sim 3$ seems consistent with the six points given above, and is just consistent with the observed jet-to-counterjet brightness ratios. A Lorentz factor of $\Gamma \sim 3$ is also consistent with the fastest apparent speeds given in Table 4 (except for the very slow speeds in Mrk 421 and 1ES 1959+650), and yields reasonable viewing angles of $2°$ to $8°$ for the apparent speeds between $0.5c$ and $2c$. It is not surprising that these viewing angles may be substantially less than $1/\Gamma$, since these sources were selected based on their TeV emission, which may have a narrower beaming cone.

The crucial questions then become: where is the parsec-scale radio emission located relative to the site of the gamma-ray emission, and what causes its lower Lorentz factor? One possibility is that the parsec-scale radio emission (at light-year scales) is located downstream of the gamma-ray emission (at light-day scales), and that the jet decelerates as it moves out. Georganopoulos & Kazanas (2003) considered such a jet that decelerates along its length and showed that the required values of the Doppler factor in the inner jet are not as high as in the homogeneous models discussed above, because the fast inner portion of the jet can more efficiently upscatter blueshifted synchrotron photons from the slower outer portion. Thus, allowing an inhomogeneous model reduces some of the apparent conflict. Wang et al. (2004) modeled a decelerating jet in which the dissipated kinetic energy of the jet is transferred to electron acceleration; they then used the resulting radiation from the accelerated electrons to successfully model the SED of several TeV blazars. Bicknell et al. (2005) have also modeled parsec-scale TeV blazar jet deceleration that they claim physically reflects a conversion of kinetic luminosity to enthalpy flux, and concluded that such deceleration can be physically consistent with the conservation of energy and momentum in this region.

A second possibility is that the jet has an inhomogeneous structure transverse to the jet axis, consisting of a fast "spine" that dominates the high-energy emission and a slower "layer" that dominates at lower frequencies, although such a structure is not mutually exclusive with the decelerating jet discussed above. For example, Ghisellini et al. (2005) proposed a jet with an initial *transverse* velocity structure consisting of a fast spine and a slow layer, and by taking into account the inverse Compton radiation each portion produced from the seed radiation coming from the other portion, they found that the resulting anisotropic inverse Compton emission from the spine may serve to decelerate it. Henri & Saugé (2006) propose a two-flow model, consisting of a mildly relativistic outer MHD jet and a central pair-plasma jet accelerated by the so-called "Compton rocket" effect to higher velocities of order $\Gamma \sim 3$. Regardless of their origin, such transverse structures may show an observational signature in the VLBI images of jets that are resolved in the transverse direction, in the form of limb brightening or limb darkening, according to which region is dominating the radio emission. Observational signatures

of limb brightening have been claimed in the VLBI images of the TeV sources Mrk 501 (Giroletti et al. 2004b), Mrk 421 (Giroletti et al. 2006), and M87 (Kovalev et al. 2007). We also found some observational evidence of limb brightening in the Mrk 421 jet (Piner & Edwards 2005), but it was present in only some of the transverse slices, suggesting a more complex transverse emission pattern on the scales that we investigated. The jets of the three fainter (in the radio) TeV sources considered in this paper are not detected with sufficient resolution or dynamic range in the VLBA images to discern structure transverse to the jet axis; those observations must be left to the brighter sources (or to much more sensitive images of these sources).

A third possibility, that the gamma-ray emission is cospatial with the parsec-scale jet knots, was suggested by observations of knot HST-1 in M87 (recently reviewed by Harris et al. 2008). That knot, lying at a distance of $\sim$100 pc from the core of M87, would lie at angular separations of a few mas from the core in the $z \sim 0.1$ TeV blazars, taking into account likely projection effects in jets with viewing angles of a few degrees. That would put features like HST-1 in M87 cospatial with the VLBI model components in the jets of the TeV blazars. If the high-energy emission is occurring in these components, that makes the different Lorentz factors and Doppler factors derived in the radio and the gamma ray particularly challenging to explain.

4.2. Pattern Speeds Unrelated to Bulk Speeds

Many sources in large VLBI surveys display a mix of stationary and moving components—but what we mean here is that even the *fastest* measured apparent pattern speed in a source may still be much less than the bulk apparent speed. The study of the 2 cm and MOJAVE survey apparent speeds (Cohen et al. 2007) found that a small fraction (about 25%) of the powerful sources showed *only* slow apparent pattern speeds that were unrelated to their bulk apparent speeds based on statistical arguments (otherwise they would have unreasonably small angles to the line of sight, or unreasonably high intrinsic luminosities). If the bulk Lorentz factor is indeed high in the parsec-scale jets of the TeV HBLs, then the fraction of these sources that have apparent pattern speeds much less than their apparent bulk speed is closer to 100%.

Is there then some plausible physical difference in the high- and low-power jets that could cause the high-power jets to form patterns that move at the bulk speed while the low-power jets do not? A common model for particle acceleration and the formation of VLBI components is the shocked-jet model (e.g., Spada et al. 2001). If such rapidly moving shocks were forming and propagating to the parsec scale in the TeV HBLs, then we might expect them to be visible in the VLBA monitoring, but they are not. Krawczynski (2007) has suggested a model in which particle acceleration in the low-power sources occurs through acceleration of parallel electron-positron or electron-proton beams rather than through shock acceleration. If a source does not form strong moving shocks, then its more continuous jet may be modeled by a series of stationary Gaussians even though the plasma is moving relativistically. Other features that are due to standing shocks, or to points where the jet bends toward the line of sight, may also appear in jets as stationary regions of locally enhanced emission, as they do in high-power sources.

Another possible physical difference between the high- and low-power jets that may cause such a difference in pattern speeds is the opening angle of the (presumably conical) jet. This possibility is explored in a series of papers by Gopal-Krishna et al. (2004, 2006, 2007). According to these models, if the low-power sources have jets with considerably larger opening angles

(Gopal-Krishna et al. 2007), then what is seen in the VLBI observations is a set of observables that have been unintentionally averaged over different viewing angles, with the small viewing-angle portion of the jet being the most Doppler boosted, and contributing the most to the weighted average. In that case, many sources may show slow apparent speeds typical of being viewed almost end-on, while the apparent speed *on the axis* of the jet is actually much higher. However, in all of the versions of this model that produce subluminal effective apparent speeds, the effective Doppler factor remains quite high ($\delta_{eff} \gtrsim 20$; see Figs. 3 and 4 of Gopal-Krishna et al. 2007), so that this model cannot easily explain the relatively low Doppler factors measured for the TeV blazars in the radio as discussed in points (a) through (f) in § 4.1 (in fact, it would predict high values for the radio variability, brightness temperature, core dominance, and inverse Compton Doppler factors).

Whether or not the opening angle has a significant effect on the observables hinges on the actual value of the opening angle—the effect is small for $1°$ opening angles and quite pronounced at $5°$ opening angles; but, perversely, measurements of blazar jet opening angles are of little use in testing the model, because the measurements of the opening angle are themselves affected by averaging over the true opening angle (see Fig. 3 of Gopal-Krishna et al. 2006). However, if the opening angles are large enough to cause a significant effect, it would seem that a substantial number of sources may be expected to have core-halo type morphology on their VLBI images (whenever the opening angle is larger than the axis viewing angle), so it would be useful to compare simulated VLBI images from this model with observed morphologies. The model also makes specific statistical predictions, e.g., that a small fraction of TeV blazars should show strongly superluminal motions (Gopal-Krishna et al. 2006), so that as the number of TeV blazars increases, it will be possible to test the observations against probability curves derived from this model.

Based on all of the available observational data, we favor a combination of possibilities 1 and 2 given at the beginning of this discussion section. From all of the other arguments for a low Lorentz factor for the parsec-scale radio emission given above (points *a* through *f* in § 4.1), we consider it likely that the parsec-scale radio-emitting region in the TeV HBLs has a substantially lower Lorentz factor than is usually derived for the high-energy gamma-ray–emitting region. A parsec-scale Lorentz factor of about 3 is indeed consistent with the peak apparent speeds of $0.5c$–$2c$ in Table 4, assuming these reflect the bulk apparent speed on the axis of the jet. However, the apparent speeds in two of the TeV blazars (Mrk 421 and 1ES 1959+650) are so low that they likely represent a subsample of these sources for which the measured pattern speeds are much less than the bulk speed, as was also found for powerful sources by Cohen et al. (2007). The physical cause of this Lorentz factor difference between the high- and low-frequency–emitting regions (and whether any Lorentz factor gradient occurs along the jet, transverse to the jet, or both) and the physical cause of any decoupling of pattern and bulk speeds has not been definitively determined, but the sample of TeV blazars is growing rapidly, so the observational statistics will improve markedly over the next several years.

5. CONCLUSIONS

We have presented new multi-epoch VLBI images for the three TeV blazars H1426+428, 1ES 1959+650, and PKS 2155−304 obtained during the years 2001–2004. The results for H1426+428 are the first multi-epoch VLBI results to be presented for this source. The results for 1ES 1959+650 and PKS 2155−304 are

combined with earlier results for these sources from Paper I to yield a longer time baseline for measurement. The major observational findings for these three sources are as follows.

1. H1426+428's parsec-scale structure during this time range was well modeled by a ~17 mJy core and a single ~3 mJy jet component at a position angle of approximately −25°, with an apparent speed of $2.09c \pm 0.53c$.

2. 1ES 1959+650 consisted of a compact core and a nearby stationary ($0.00c \pm 0.04c$) jet component at a position angle of about 125° and a separation of about 0.35 mas at 15 GHz. On larger scales of a few mas the jet is diffuse and directed to the north, so that this source shows an extreme apparent misalignment of about 130° on parsec scales.

3. PKS 2155−304 was observed with dual-circular polarization at 15 GHz. The fractional polarization at the position of the core was 3%, and the electric vector position angle was 131°, about 30° misaligned from the innermost jet position angle. The measured apparent speed of the single jet component was $0.93c \pm 0.31c$.

We combined the new apparent speed measurements from this paper with the apparent speeds measured in TeV blazar jets from our earlier papers to form a current set of apparent speed measurements in TeV HBLs (Table 4). The mean peak apparent pattern speed in the jets of the TeV HBLs is about $1c$. The statistical result noted in Paper I that the TeV HBLs have significantly slower apparent jet pattern speeds compared to radio-selected or GeV-selected blazars is strengthened by the new results of this paper. Section 4 presents a thorough analysis of these results in the context of other radio observations and theoretical models for TeV blazar jets. Conclusions from that analysis are as follows.

1. The peak apparent speeds of order $0.5c$–$2c$ in four of the six studied TeV blazars (Table 4), when taken together with other observed radio properties discussed in § 4, are consistent with radio jets with bulk Lorentz factors of $\Gamma \sim 3$ and viewing angles of a few degrees.

2. The very slow peak apparent speeds in two of the six studied TeV blazars in Table 4 (Mrk 421 and 1ES 1959+650) are likely pattern speeds that are unrelated to the bulk apparent speeds of the jets, which are likely to be similar to those mentioned above.

Facilities: VLBA

REFERENCES

Aharonian, F., et al. 2002, A&A, 384, L23
———. 2003, A&A, 403, 523
———. 2005a, A&A, 430, 865
———. 2005b, A&A, 442, 895
———. 2007, ApJ, 664, L71
Alberdi, A., Marcaide, J. M., Marscher, A. P., Zhang, Y. F., Elosegui, P., Gomez, J. L., & Shaffer, D. B. 1993, ApJ, 402, 160
Albert, J., et al. 2006, ApJ, 639, 761
Aller, M. F., Aller, H. D., & Hughes, P. A. 2006, in ASP Conf. Ser. 350, Blazar Variability Workshop II: Entering the *GLAST* Era, ed. H. R. Miller et al. (San Francisco: ASP), 25
Bennett, C. L., et al. 2003, ApJS, 148, 1
Bicknell, G. V., Safouris, V., Saripalli, L., Saxton, C. J., Subrahamanyan, R., Sutherland, R. S., & Wagner, S. J. 2005, in AIP Conf. Proc. 745, High Energy Gamma-Ray Astronomy: 2nd International Symposium, ed. F. A. Aharonian, H. J. Völk, & D. Horns (New York: AIP), 140
Bondi, M., Marcha, M. J. M., Dallacasa, D., & Stanghellini, C. 2001, MNRAS, 325, 1109
Bondi, M., Marcha, M. J. M., Polatidis, A., Dallacasa, D., Stanghellini, C., & Anton, S. 2004, MNRAS, 352, 112
Böttcher, M. 2005, ApJ, 621, 176 (erratum 641, 1233 [2006])
Chiaberge, M., Celotti, A., Capetti, A., & Ghisellini, G. 2000, A&A, 358, 104
Cohen, M. H., Lister, M. L., Homan, D. C., Kadler, M., Kellermann, K. I., Kovalev, Y. Y., & Vermeulen, R. C. 2007, ApJ, 658, 232
Costamante, L., Aharonian, F., Ghisellini, G., & Horns, D. 2003, NewA Rev., 47, 677
Costamante, L., et al. 2001, A&A, 371, 512
Daniel, M. K., et al. 2005, ApJ, 621, 181
Djannati-Ataï, A., et al. 2002, A&A, 391, L25
Dodson, R., et al. 2008, ApJS, 175, 314
Edwards, P. G., & Piner, B. G. 2002, ApJ, 579, L67
Falcone, A. D., Cui, W., & Finley, J. P. 2004, ApJ, 601, 165
Fossati, G., et al. 2008, ApJ, 677, 906
Georganopoulos, M., & Kazanas, D. 2003, ApJ, 594, L27
Ghisellini, G., Celotti, A., & Costamante, L. 2002, A&A, 386, 833
Ghisellini, G., Tavecchio, F., & Chiaberge, M. 2005, A&A, 432, 401
Giovannini, G., Giroletti, M., & Taylor, G. B. 2008, in ASP Conf. Ser., Extragalactic Jets: Theory and Observation from Radio to Gamma Ray, ed. T. A. Rector & D. S. De Young (San Francisco: ASP), in press (arXiv: 0708.3911v1)
Giroletti, M., Giovannini, G., Taylor, G. B., & Falomo, R. 2004a, ApJ, 613, 752

Giroletti, M., Giovannini, G., Taylor, G. B., & Falomo, R. 2006, ApJ, 646, 801
Giroletti, M., et al. 2004b, ApJ, 600, 127
Gopal-Krishna, Dhurde, S., Sircar, P., & Wiita, P. J. 2007, MNRAS, 377, 446
Gopal-Krishna, Dhurde, S., & Wiita, P. J. 2004, ApJ, 615, L81
Gopal-Krishna, Wiita, P. J., & Dhurde, S. 2006, MNRAS, 369, 1287
Gutierrez, K., et al. 2006, ApJ, 644, 742
Harris, D. E., Cheung, C. C., Stawarz, L., Biretta, J. A., Sparks, W., Perlman, E. S., & Wilson, A. S. 2008, in ASP Conf. Ser., Extragalactic Jets: Theory and Observation from Radio to Gamma Ray, ed. T. A. Rector & D. S. De Young (San Francisco: ASP), in press (arXiv: 0707.3124v1)
Henri, G., & Saugé, L. 2006, ApJ, 640, 185
Horan, D., et al. 2002, ApJ, 571, 753
Jorstad, S. G., Marscher, A. P., Mattox, J. R., Wehrle, A. E., Bloom, S. D., & Yurchenko, A. V. 2001, ApJS, 134, 181
Kato, T., Kusunose, M., & Takahara, F. 2006, ApJ, 638, 653
Kellermann, K. I., et al. 2004, ApJ, 609, 539
Kollgaard, R. I., Gabuzda, D. C., & Feigelson, E. D. 1996, ApJ, 460, 174
Königl, A. 1981, ApJ, 243, 700
Kovalev, Y. Y., Lister, M. L., Homan, D. C., & Kellermann, K. I. 2007, ApJ, 668, L27
Kovalev, Y. Y., et al. 2005, AJ, 130, 2473
Krawczynski, H. 2007, ApJ, 659, 1063
Krawczynski, H., et al. 2004, ApJ, 601, 151
Kusunose, M., & Takahara, F. 2006, ApJ, 651, 113
Laurent-Muehleisen, S. A., Kollgaard, R. I., Moellenbrock, G. A., & Feigelson, E. D. 1993, AJ, 106, 875
Lister, M. L. 2006, in ASP Conf. Ser. 350, Blazar Variability Workshop II: Entering the *GLAST* Era, ed. H. R. Miller et al. (San Francisco: ASP), 139
Lovell, J. E. J. 2000, in Astrophysical Phenomena Revealed by Space VLBI, ed. H. Hirabayashi, P. G. Edwards, & D. W. Murphy (Sagamihara: ISAS), 301
Ma, C., et al. 1998, AJ, 116, 516
Mutel, R. L., & Denn, G. R. 2005, ApJ, 623, 79
Petry, D., et al. 2002, ApJ, 580, 104
Piner, B. G., & Edwards, P. G. 2004, ApJ, 600, 115 (Paper I)
———. 2005, ApJ, 622, 168
Piner, B. G., Mahmud, M., Fey, A. L., & Gospodinova, K. 2007, AJ, 133, 2357
Piner, B. G., Unwin, S. C., Wehrle, A. E., Edwards, P. G., Fey, A. L., & Kingham, K. A. 1999, ApJ, 525, 176
Rector, T. A., Gabuzda, D. C., & Stocke, J. T. 2003, AJ, 125, 1060

Sakamoto, Y., et al. 2008, ApJ, 676, 113
Simard-Normandin, M., Kronberg, P. P., & Button, S. 1981, ApJS, 45, 97
Spada, M., Ghisellini, G., Lazzati, D., & Celotti, A. 2001, MNRAS, 325, 1559
Stirling, A. M., et al. 2003, MNRAS, 341, 405
Urry, C. M., & Padovani, P. 1995, PASP, 107, 803
Wagner, R. 2008a, MNRAS, 385, 119
———. 2008b, in ASP Conf. Ser., Extragalactic Jets: Theory and Observation from Radio to Gamma Ray, ed. T. A. Rector & D. S. De Young (San Francisco: ASP), in press (arXiv: 0706.4439v1)

Wang, J., Li, H., & Xue, L. 2004, ApJ, 617, 113
Wolter, A., Beckmann, V., Ghisellini, G., Tavecchio, F., Maraschi, L., Costamante, L., Celotti, A., & Ghirlanda, G. 2008, in ASP Conf. Ser., Extragalactic Jets: Theory and Observation from Radio to Gamma Ray, ed. T. A. Rector & D. S. De Young (San Francisco: ASP), in press (arXiv: 0707.2735v1)
Zavala, R. T., & Taylor, G. B. 2003, ApJ, 589, 126
———. 2004, ApJ, 612, 749